Cellular Microbiology (2008) **10**(10), 2012–2028
doi:10.1111/j.1462-5822.2008.01184.x
First published online 8 July 2008

The unique architecture of Bunyamwera virus factories around the Golgi complex

Juan Fontana,[1] Noelia López-Montero,[1] Richard M. Elliott,[2] José Jesús Fernández[3] and Cristina Risco[1]*

[1]*Cell Structure Laboratory, Centro Nacional de Biotecnología, CSIC, Campus Universidad Autónoma, Cantoblanco, 28049 Madrid, Spain.*
[2]*Centre for Biomolecular Sciences, School of Biology, University of St Andrews, UK.*
[3]*Departamento de Arquitectura de Computadores, Universidad de Almería, Spain.*

Summary

Viral factories are novel structures built by viruses in infected cells. During their construction organelles are recruited and build a large scaffold for viral replication and morphogenesis. We have studied how a bunyavirus uses the Golgi to build the factory. With the help of confocal and 3D ultrastructural imaging together with molecular mapping *in situ* and *in vitro* we have characterized a tubular structure that harbours the viral replication complexes in a globular domain. Numerous ribonucleoproteins were released from purified tubes disrupted *in vitro*. Actin and myosin I were identified by peptide mass fingerprinting in isolated tubes while actin and the viral NSm non-structural protein were detected in the tubes' internal proteinaceous scaffold by immunogold labelling. Studies with NSm deletion mutants and drugs affecting actin showed that both NSm and actin are key factors for tube and virus assembly in Golgi. Three-dimensional reconstructions based on oriented serial sections of infected cells showed that tubes anchor cell organelles to Golgi stacks and make contacts with intracellular viruses. We propose that this new structure, unique among enveloped viruses, assembles in association with the most stable component of Golgi stacks, the actin-containing matrix scaffold, connecting viral replication and morphogenesis inside viral factories.

Received 12 May, 2008; accepted 29 May, 2008. *For correspondence. E-mail crisco@cnb.csic.es; Tel. (+34) 915 854 507. Fax (+34) 915 854 506.

Introduction

RNA viruses replicate their genome in intracellular membranes of infected cells (Mackenzie, 2005; Salonen *et al*., 2005). Modified membranes harbouring viral replication complexes (RCs) frequently integrate into a complex structure known as the 'viral factory' where the cytoskeleton participates, cell organelles are recruited and the different steps of the virus life cycle are sequentially connected. Characterizing how this happens would help to understand how viral factors take control of cells and modify their architecture. There is no description of the mechanisms involved in the formation of most viral factories, although there is evidence that some viruses induce aggresomes and autophagosomes to generate sites of replication (Novoa *et al*., 2005a; Wileman, 2006). Expression of early proteins such as viral polymerases is probably sufficient to program the cell for organelle recruitment and factory formation, as recently observed in cells transfected with rubella virus replicons (Fontana *et al*., 2007).

The viral replication machinery is usually inserted in single- or double-membrane vesicles that can be associated with a variety of organelles, such as the rough endoplasmic reticulum (RER), mitochondria, the endolysosomal system and chloroplasts or vacuolar membranes in plants (Hagiwara *et al*., 2003; Novoa *et al*., 2005a; Salonen *et al*., 2005; Kopek *et al*., 2007). Some viruses, e.g. polioviruses, induce proliferation of specific membranes creating a 'novel compartment' (Cherry *et al*., 2006) where the viral RNA polymerase molecules can assemble bidimensional arrays (Hobson *et al*., 2001; Lyle *et al*., 2002). Although the purpose of this targeted localization has not been elucidated, one possibility is that association of RCs with membranes provides a structural framework for efficient replication and transfer of replicated RNA to assembly sites in contiguous membranes.

Bunyaviruses comprise a large family of RNA enveloped viruses that includes serious emergent pathogens for humans, animals and plants, and are responsible for severe episodes of encephalitis and haemorrhagic fevers in humans (Elliott, 1997). They assemble a large factory involving the Golgi complex where virus particles bud and mature (Salanueva *et al*., 2003; Novoa *et al*., 2005b). Bunyamwera virus (BUNV) serves as a model for the many pathogens within this family. It contains three RNA segments of negative-sense polarity. The large segment

(L) codes for an RNA-dependent RNA polymerase (L protein), the medium segment (M) codes for a precursor polyprotein (NH_2-Gn-NSm-Gc-COOH), which is cotranslationally cleaved to yield the two virion glycoproteins (Gn and Gc) and a non-structural protein called NSm, and the smallest segment (S) codes for the nucleoprotein N and a second non-structural protein NSs in overlapping reading frames (Elliott, 1990). The NH_2-terminal domain of NSm is essential for BUNV morphogenesis (Shi *et al*., 2006) while NSs is a non-essential protein that contributes to viral pathogenesis (Bridgen *et al*., 2001). There is no ultrastructural description of the bunyavirus replication site that has been defined as 'cytoplasmic' (Nichol *et al*., 2005).

Morphogenesis of coronaviruses, arteriviruses, rubiviruses and bunyaviruses is associated to the Golgi complex. The choice of the Golgi for viral replication or assembly is somehow surprising. The Golgi is a highly dynamic organelle whose function requires continual membrane and protein flow (James Morre and Mollenhauer, 2007). On the other hand, the Golgi may be an autonomous organelle with a stable framework (Seemann *et al*., 2000). Its unique architecture is thought to depend on cytoplasmic matrix proteins and the cytoskeleton. Actin seems to participate in the preservation of the flattened shape of Golgi cisternae (Lazaro-Dieguez *et al*., 2006) and several actin-binding proteins are known to play some role in Golgi function. These include myosins and spectrins (Beck, 2005).

We have studied how a bunyavirus modifies cell structure and builds factories around the Golgi complex from early to late steps of its life cycle. In a previous study we observed that Golgi stacks contain peculiar virus-induced tubular structures in BUNV-infected cells (Salanueva *et al*., 2003). With the help of three-dimensional reconstructions and molecular mapping *in situ* and *in vitro* we have characterized these tubular elements and discovered that they represent a new structure of viral and cellular origin. Tubes assemble in Golgi stacks where they seem to be involved in multiple functions including viral genome replication, transfer of viral ribonucleoprotein complexes to assembly sites and viral morphogenesis. We propose that this new multifunctional structure associates with the actin-containing matrix of the Golgi stacks providing a stable scaffold for viral replication and early morphogenesis.

Results

Cell architecture is deeply modified early in infection

Changes in cell organization during assembly of the viral factory were studied by confocal microscopy (Fig. 1). Control monolayers (Fig. 1A) showed round-shaped nuclei (blue), perinuclear Golgi elements (red) and well-defined straight actin stress fibres (green). Infected cells (Fig. 1B) have a completely different aspect: nuclei are elongated, the Golgi is rounded and concentrates on one side of the nucleus, and stress fibres have moved to the cell periphery. No changes in microtubules or vimentin filaments were observed (not shown). In addition to the WGA *trans*-Golgi marker shown in Fig. 1A and B, two additional Golgi markers (giantin and galactosyltransferase or Gal-T) exhibited a similar transition from a perinuclear distribution in non-infected cells (Fig. 1C and D) to a more compact pattern on one side of the nucleus in infected cells (Fig. 1E and F). When observing just nuclei-associated staining a depression was frequently detected, corresponding to the location of the viral factory (Fig. 1G and H). Electron microscopy (EM) showed factories as groups of organelles near the nucleus (Fig. 1I). Higher magnifications showed round-shaped and tubular structures in Golgi stacks (Fig. 1J and K). We have detected these structures in several mammalian cultured cell types that support bunyavirus replication such as BHK-21 (this study), Vero (Salanueva *et al*., 2003) and CHO cells (not shown). Their number was higher early in infection and their viral origin was demonstrated in previous studies (Salanueva *et al*., 2003). In the present work we have studied a large number of serial sections and discovered that viral tubes actually contain a tubular domain and a bigger globular domain on one of the extremities (Fig. 1L). The tubes are open to the cytoplasm (arrows in Fig. 1K–M).

Golgi tubular structures contain the replication complexes of the virus and interact with mitochondria

BUNV generates round-shaped and tubular structures in infected cells whose representative views in thin sections of epoxy resin are summarized in Fig. 2A–H. The Golgi-associated morphogenetic pathway of BUNV and the structural and biochemical characterization of the three viral forms have been previously described in detail (Salanueva *et al*., 2003; Novoa *et al*., 2005a,b). Global understanding of all these structures has been possible through a careful analysis of consecutive serial sections (see below). Condensation of material in individual Golgi sacculi originates arcs opened to the cytosol (Fig. 2A), elongated globular structures of low internal electron-density (Fig. 2B) and complete viral tubes with both globular and cylindrical domains (Fig. 2C). The two types of cross-sections originated by a viral tube are shown in Fig. 2D and E. Cross-sectioned globular heads are always > 100 nm in diameter and most of these structures have a diameter of 120–150 nm. The cylindrical domain of viral tubes has a cross-section of 80–100 nm in diameter. Virus particles have smaller diameters (Fig. 2F–H).

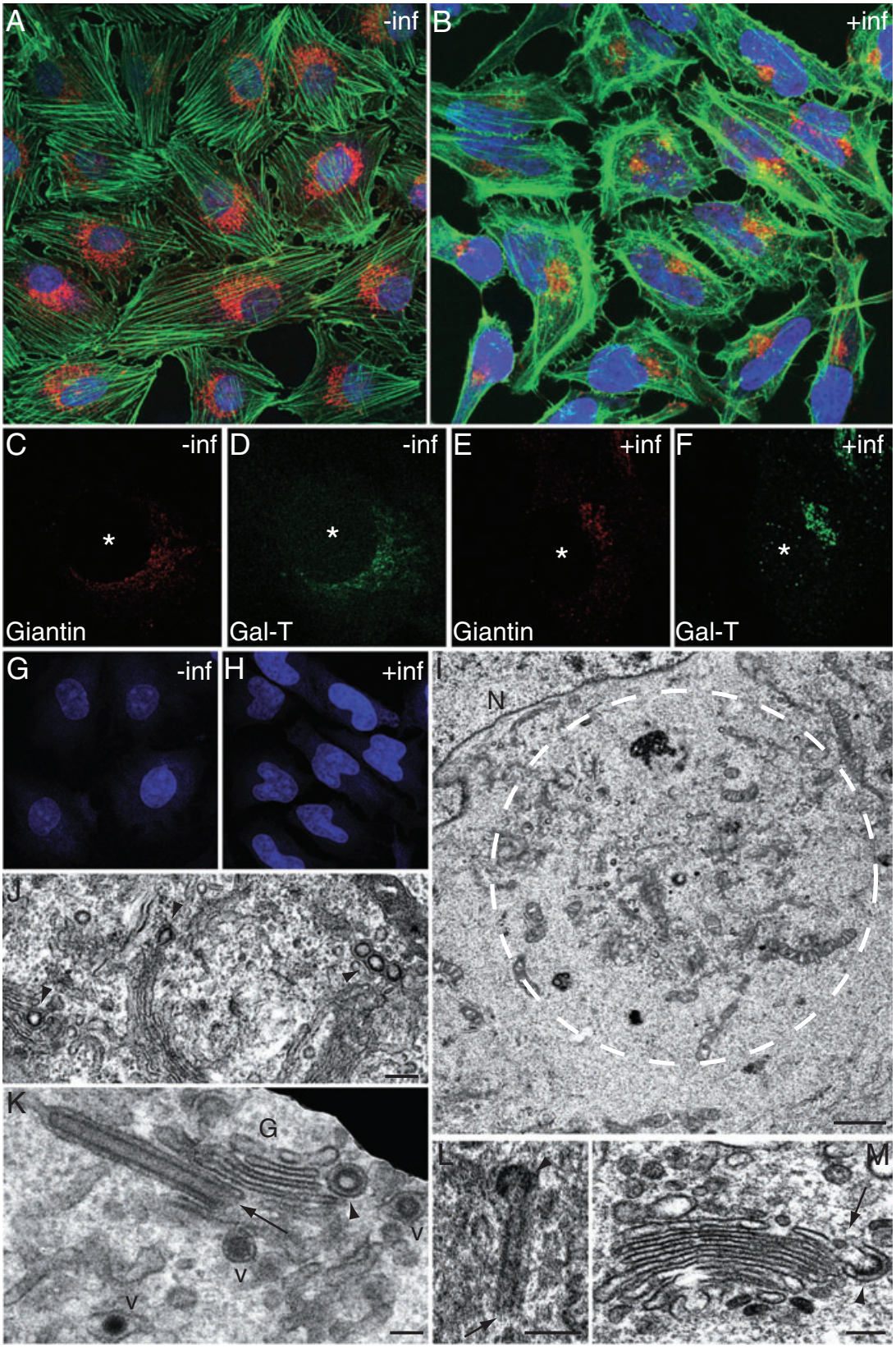

Budding profiles in Golgi membranes generate immature viruses or VI that are released into the lumen of a Golgi sacculus (Fig. 2F). Intermediate intracellular virus or VII exits the Golgi in secretory vesicles (Fig. 2G) and mature extracellular virions or VE are seen in the extracellular environment (Fig. 2H). All three viral forms have a diameter of around 70 nm in thin sections of epoxy resin for ultrastructural studies. In cryosections for immunogold detection of specific components structural details of viral tubes and viruses change (Fig. 2I–L). Diameter of sectioned viruses is around 65 nm while the globular domain of the viral tube is around 100–130 nm. Unequivocal views of the cylindrical domain of viral tubes are not easily obtained in cryosections. Specific labelling with the Golgi marker giantin confirmed that the viral tubes are associated to Golgi stacks (Fig. 2I). Viral polymerase L (Pol) and nucleocapsid N (Nuc) proteins are present in these globular domains as detected by immunogold labelling and EM (Fig. 2J–L). N also accumulates around Golgi membranes (Fig. 2L) while L concentrates in an internal layer of the tube globular domain (Fig. 2K). Double-stranded RNA (dsRNA), an intermediate of RNA replication (Fig. 2M and N) as well as incorporated BrUTP (Fig. 2O and P) locate in the globular domain of viral tubes according to immunogold labelling. These data strongly suggest that the globular domain of viral tubes harbours the BUNV RCs. Confocal microscopy showed RCs attached to recruited mitochondria (Fig. 2Q) and EM shows that tubes contact and sometimes fuse with the external mitochondrial membrane (Fig. 2R–T).

Isolated tubes contain RC components and RNPs

Cell fractionation and centrifugation in Optiprep gradients allowed isolation of viral tubular structures (Fig. 3A). Negative staining confirmed their general morphology: they contain a cylindrical and a globular domain (Fig. 3B and C) similar to tubes *in situ* (Fig. 1L) and a filamentous internal texture (Fig. 3D). dsRNA was detected in isolated tubes by dot-blot (Fig. 3E). Viral proteins involved in genome replication such as the RNA Pol and the Nuc protein were detected by Western blot and Coomasie blue staining, respectively (Fig. 3F). Controlled disruption of isolated tubes by saponin treatment showed a proteinaceous internal scaffold (Fig. 3G) that was labelled with anti-Pol and anti-Nuc antibodies (Fig. 3H and I). Complete disruption of tubes provoked the release of viral ribonucleoprotein complexes or RNPs (Fig. 3J). Similar release of RNPs was observed when disrupting isolated viruses *in vitro* (Novoa *et al*., 2005b).

The viral non-structural NSm protein in tubular structures

NSm is a transmembrane non-structural protein involved in BUNV morphogenesis (Shi *et al*., 2006) that accumulates in the Golgi region of infected cells (Lappin *et al*., 1994; Shi *et al*., 2006). Immunogold and EM showed that NSm localizes both in the cylindrical (Fig. 4A and B) and globular (Fig. 4C) domains of Golgi-associated viral tubes. NSm was detected in Golgi membranes where new virus particles are assembling (Fig. 4D). Western blot analysis confirmed the presence of NSm in isolated viral tubes and intracellular viral intermediates I and II while extracellular mature virions lacked the protein (Fig. 4E). The same result was obtained by immunogold detection of NSm and EM of isolated viruses disrupted *in vitro* (not shown). This distribution is typical for the behaviour of scaffolding proteins that assist in the assembly of immature viral precursors and are later degraded by proteolysis during maturation (Steven *et al*., 2005). To obtain functional information about the role of NSm in viral tubes and viral particles three NSm mutants were characterized at the ultrastructural level (Fig. 4F–H). These viruses obtained by a reverse genetics approach have deletions in NSm domains III and IV (Shi *et al*., 2006). They grow slowly generating maximum virus yields 10- to 100-fold lower than wild-type BUNV. When studying ultrathin sections of cells infected with NSmΔ4 mutant virus, viral tubes were rarely seen. More than 200 cells infected with wild-type BUNV and an equivalent amount of cells infected with NSmΔ4 mutant virus at 6, 10 and 24 h post infection (p.i.) were studied by oriented serial sectioning. While more than 50 viral tubes per cell were detected when infecting with the wild-type virus, a total of 12 complete tubes (longitudinal sections of the cylindrical domain) were seen in ~200 cells infected with the mutant virus. Tubes assembled by the NSm mutant were appar-

Fig. 1. Visualization of viral factories by confocal and electron microscopy.
A–H. Control (A) and bunyavirus-infected (B) BHK-21 cells were labelled for *trans*-Golgi detection (WGA, red), actin (Phallodin, green) and nuclei (To-Pro, blue) at 8 h p.i. Localization of giantin and Gal-T Golgi markers in control (C and D) and infected cells (E and F). (G) and (H) show nuclear shape in control and infected cells. Z-series projections of single optical sections are shown in (A–H).
I. Electron microscopy of viral factories shows groups of organelles near the nucleus (dashed white circle).
J. Higher magnifications of Golgi stacks in factories show globular structures of low internal electron-density (arrowheads) as well as longitudinal (arrow) and transversal (arrowhead) sections of tubular structures (K). Viral particles (V) are also seen.
L. Tubular element with elongated (arrow) and globular (arrowhead) domains.
M. Tube in a Golgi stack with an opening (arrow) near the globular domain (arrowhead). N, nucleus. Bars: 1 μm in I; 200 nm in J; 100 nm in K–M.

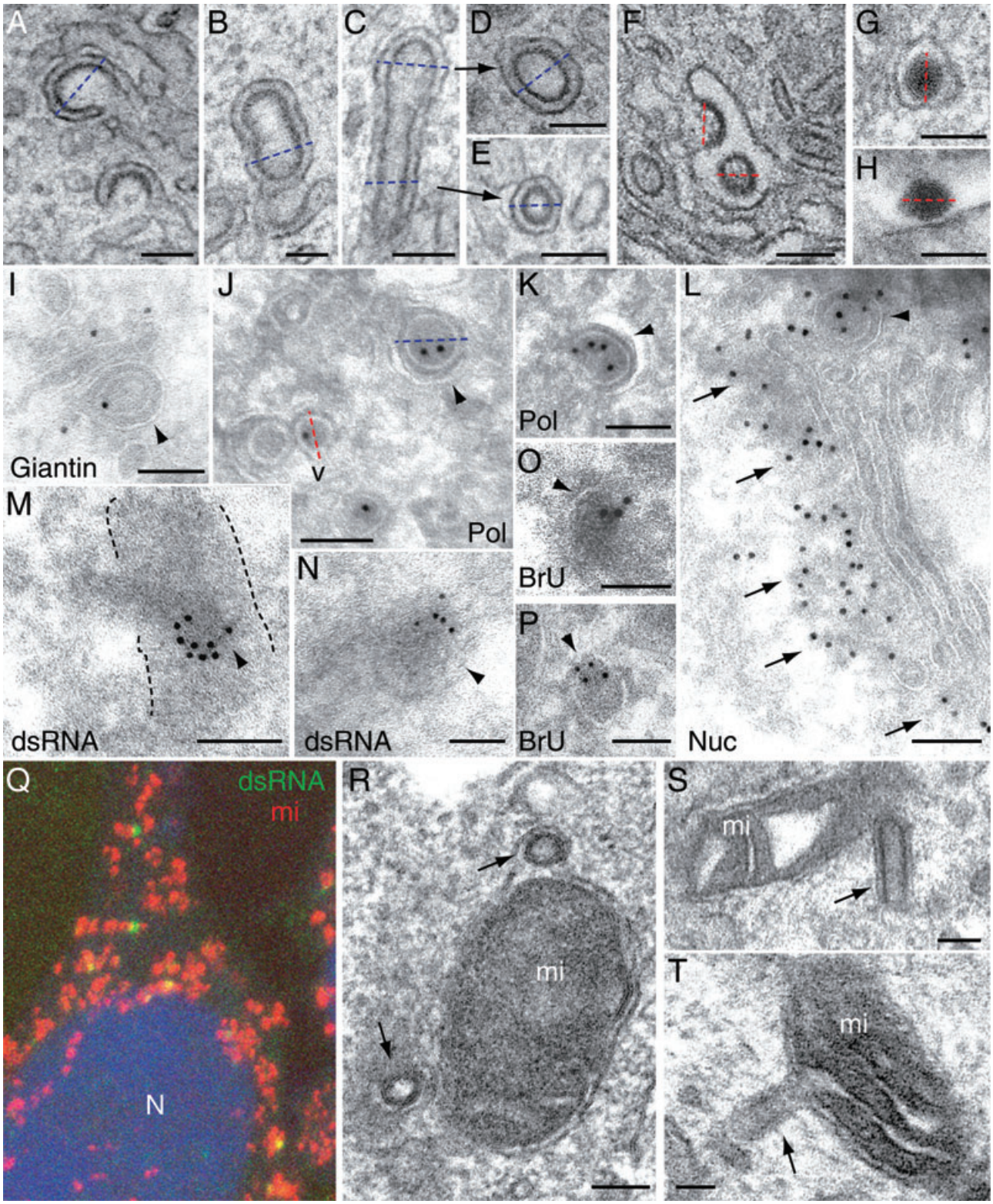

ently less rigid than normal, had small heads and exhibited a diameter of 60–100 nm (Fig. 4F). Intracellular immature viral intermediates (type I viruses) accumulated in Golgi membranes which suggests a blockade in viral particle maturation (Fig. 4G). A significant amount of viral glycoproteins was visualized at the plasma membrane by confocal microscopy (not shown) and budding profiles were also frequently seen at the cell surface (Fig. 4H).

Fig. 2. Structural characterization of the globular domain of viral tubes. (A–H) Views generated by Bunyamwera virus structures in infected cells as studied in ultrathin sections of epoxy resin. For direct size comparison the diameter of each structure is marked with blue dashed lines on tubes and red dashed lines on viruses.
A. Arcs that originate the globular domain of viral tubes.
B. Elongated globular domain.
C. Complete tube with globular head and cylindrical domain.
D and E. Cross sections of a globular and a cylindrical domain respectively.
F. Virus budding profile and immature virus (VI) in the lumen of a Golgi sacculus.
G. Intracellular transition virus (VII).
H. Extracellular mature virion (VE).
I. Immunogold detection with the Golgi marker giantin confirms that tubes are Golgi-associated (arrowhead).
J and K. Detection of BUNV viral polymerase (L or Pol) in the globular domain of tubes (arrowheads) and viral particles (v). Dashed lines are added for a direct comparison of diameters of globular heads of tubes and intracellular viruses as visualized in cryosections. Pol-associated signal in (K) aligned under the internal layer of the globular domain of the tube.
L. Viral nucleocapsid (Nuc) is also detected in the globular domain of tubes (arrowhead) and around Golgi membranes (arrows).
M and N. Immunogold detection of dsRNA in the globular domain of tubes as visualized by freeze-substitution (arrowheads). Black dashed lines in (M) indicate the external limits of the Golgi stack where the tube is inserted.
O and P. BrU detection in globular heads of tubes (arrowheads).
Q. Confocal microscopy (Z-series projection of single optical sections) shows association of viral tubes (green) with mitochondria (red) also observed by EM (arrows in R to T). (I–L), (O) and (P) show labelling on cryosections while (M) and (N) correspond to labelling on Lowicryl sections after freeze-substitution. N, nucleus; mi: mitochondria. Bars: 100 nm in A–M, O, P, R–T; 50 nm in N.

Similar results were obtained with NSmΔ3 and NSmΔ5 deletion mutants, with small differences in the amount of intracellular virus particles and budding profiles in plasma membrane compared with NSmΔ4 virus (not shown). These data confirmed an active participation of NSm protein in tube structure and virus assembly in Golgi, and pointed to viral tubes as elements involved in viral morphogenesis.

Cellular proteins in viral tubes

Matrix-assisted laser desorption ionization (MALDI) peptide mass fingerprinting and database searching (Navarro-Lerida *et al*., 2004) was performed to detect cellular proteins in purified tubes. The highest scores obtained from this study corresponded to cytoskeleton-associated proteins (actin, myosin I and tubulin), several ribosomal proteins, the eukaryotic translation elongation factor 2 and a retinoblastoma-like protein (Table 1). Considering the filamentous internal structure of the tubes (Fig. 3D), we focused our attention on the cytoskeletal proteins. Confocal microscopy showed that although actin is mostly removed from the viral factory some spots of actin remained in the modified Golgi region (Fig. 5A). Omitting the actin and Golgi-associated signals showed a weak To-Pro blue staining that most probably corresponds to RNA accumulation in the factory (Fig. 5B). When the Golgi signal is omitted, thin filamentous elements of actin are distinguished (Fig. 5C). The dimensions of these filamentous structures are compatible with those of viral tubes as seen by EM. Actin was detected by Western blot in isolated tubes and intracellular viruses while it was absent in extracellular mature virions (Fig. 5D). Actin was also detected by immunogold labelling in tubes and viruses as shown in cryosections of infected cells (Fig. 5E and F) and on isolated tubes (Fig. 5G–I). Intact tubes exhibited a very weak or no immunogold signal (Fig. 5G), while tubes opened with saponin 'on grid' showed an enhanced signal on the released protein aggregates (Fig. 5H and I). An actin-associated signal was also detected on protein aggregates released from intracellular immature viruses disrupted *in vitro* (not shown). These results confirmed the presence of actin as a component of the internal fibres of viral tubes and its incorporation into immature viruses.

Table 1. Cell proteins identified in isolated viral tubes by MALDI peptide mass fingerprint.

Band No.	Accession No. (gi)	Protein name	Score[a]	*Mr*	Peptide matches	Sequence coverage
1	73969194	Myosin I	89	227 600	19	8%
2	6686330	Retinoblastoma-like protein 2	96	129 701	12	11%
3	26324898	Eukaryotic translation elongation factor 2	99	96 222	9	10%
4	6678469	Tubulin	77	50 562	8	23%
5	809561	Gamma-actin	94	41 335	7	21%
6	950115	Ribosomal protein S4	76	29 676	8	29%
7	58037465	Ribosomal protein L18A	74	21 004	7	39%
8	7305445	Ribosomal protein S16	66	16 460	7	37%

a. MOWSE score calculated using MASCOT search engine. Scores are significant with a *P*-value smaller than 0.05 ($P < 0.05$).
For protein identification, the non-redundant NCBI database was searched using MASCOT 2.1 (http://www.matrixscience.com). The following NrNCBI database versions were used: 20050928, 20051014, 20050429 and 20050611.

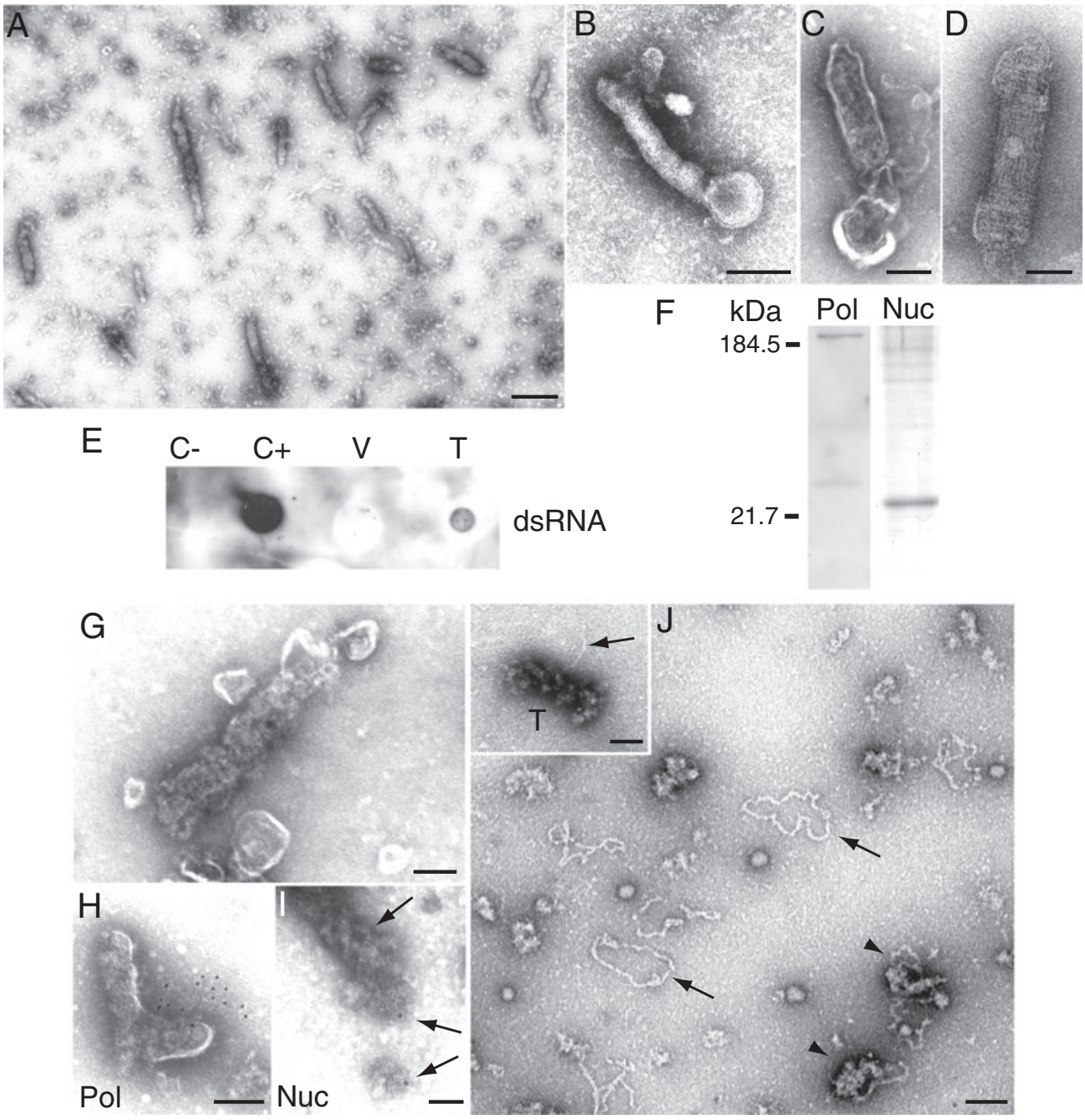

Fig. 3. Characterization of isolated tubes.
A. Negative staining of fractions enriched in viral tubes.
B. Globular and cylindrical domains are distinguished in intact tubes and in tubes submitted to a short treatment with saponin (C).
D. An internal fibrous texture is distinguished when the staining agent penetrates in the tubes.
E. Dot-blot assay shows reactivity on isolated tubes (T) with anti-dsRNA antibodies. Viral particles (V) are negative as well as a control ssRNA (C–, yeast RNA). A dsRNA virus was used as a positive control (C+).
F. Western blot detection of viral polymerase (Pol) and Coomasie blue staining corresponding to nucleocapsid (Nuc) in isolated tubes.
G. Disruption of isolated tubes with saponin shows an internal proteinaceous scaffold.
H and I. Disrupted tubes labelled with anti-Pol and anti-Nuc antibodies respectively.
J. Prolongued saponin treatment causes the complete disruption of the integrity of tubes (T) and the release of numerous RNPs (arrows in main field and inset). Arrowheads point to protein aggregates with RNPs. Bars: 300 nm in A; 100 nm in B–D, G, H and J; 50 nm in I.

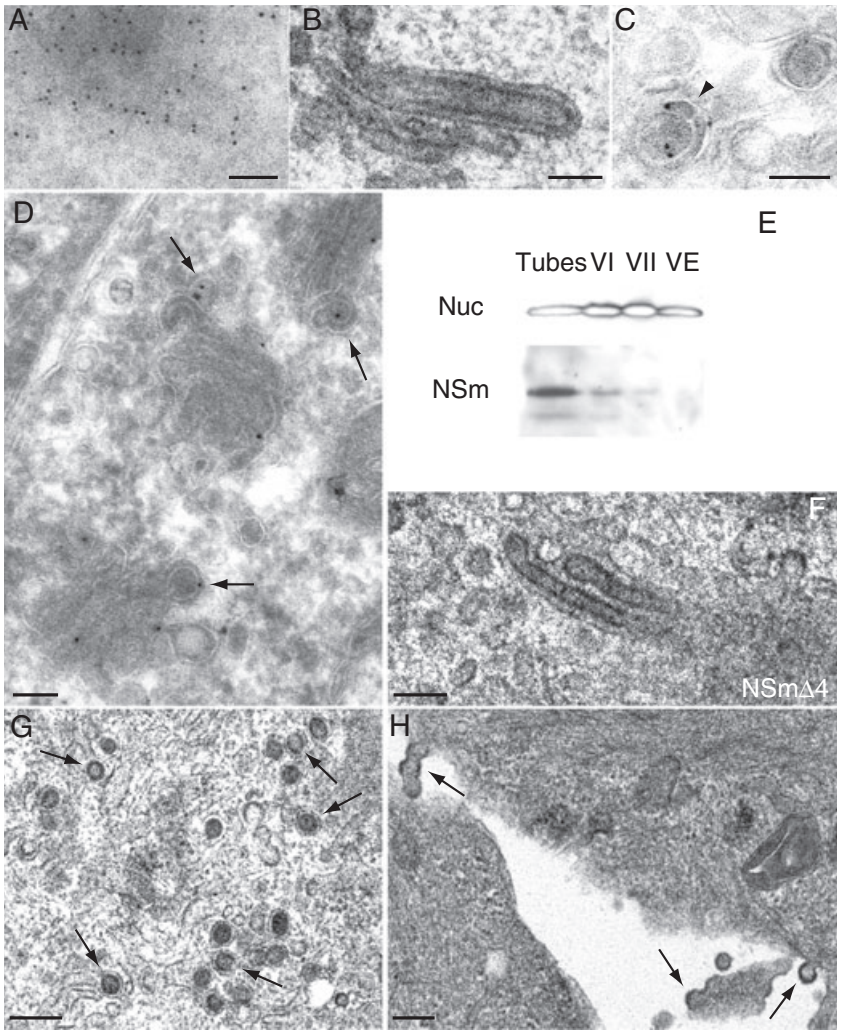

Fig. 4. Viral non-structural NSm protein and viral tubes.
A. Immunogold labelling on Lowicryl sections after freeze-substitution showing NSm in the tubular domain of a viral tube.
B. A similar tube in an epoxy-resin section is shown for comparison.
C. Labelling on cryosections also detects NSm in the globular domain of tubes and in assembling viruses in Golgi (D).
E. Western blot detection of NSm in isolated viral tubes and viral forms. Positive reaction is detected in tubes and the two intracellular viral forms (VI and VII) while no NSm is detected in extracellular virions (VE). Detection of viral nucleocapsid (Nuc) was done in the same membrane.
F. Electron microscopy shows thin tubes with small heads in BHK-21 cells infected 10 h (1 PFU/cell) with the NSmΔ4 deletion mutant that also accumulates intracellular immature VI viral particles (arrows in G).
H. Budding profiles in plasma membrane (arrows) are also abundant in these cells.
Bars: 100 nm in A–D, F; 200 nm in G and H.

Effects of brefeldin A and drugs for actin in tube integrity and virus assembly

Assembly of viral tubes in Golgi stacks could involve Golgi membrane components or more stable Golgi matrix proteins. To test these possibilities we used brefeldin A (BFA), a drug that induces the rapid fusion of Golgi membrane with pre-Golgi membranes and RER leaving a separated scaffold of matrix components (Seemann *et al*., 2000). From previous studies we knew that drugs disrupting *cis*- and *medial*-Golgi subcompartments block BUNV replication when added at 0–1 h p.i. (Salanueva *et al*., 2003; Novoa *et al*., 2005a). Thus, short BFA treatments were applied to already infected BHK-21 cells. Drug was added to the cultures at 10 h p.i., followed by immunofluorescence staining for GalT or giantin (Fig. 6A–F). At 15 or 30 min after adding BFA the immunofluorescence signal for GalT, a Golgi membrane enzyme, was rapidly fragmented and dispersed while giantin, a Golgi matrix protein, stayed in the perinuclear location for longer times. Similar effects were seen after just 5 min of treatment (data not shown). Viral tubes deprived of surrounding Golgi membranes had normal globular and cylindrical domains (Fig. 6G–I) and maintained their internal proteinaceous scaffolds and contacts with mitochondria (Fig. 6G). Tubes with apparent connections with cytoplasmic fibres that remind cytoskeletal intermediate filaments were observed (Fig. 6H). Viral tubes with short BFA treatments then exhibited the same behaviour than giantin and remained as distinguishable structures when Golgi stacks have already disappeared.

Several drugs that affect actin such as latrunculin A (LtA), cytochalasin D (CyD) and jasplakinolide (Jpk) were also used to target actin associated to Golgi membranes. Among them, the actin-stabilizing drug Jpk provided the clearest results. LtA and CyD had very little or no effect, respectively, on viral replication and assembly as determined by measurement of infectious viral particles released to the culture supernatants at 6 and 10 h p.i. Complete tubes, virus budding profiles and viral particles

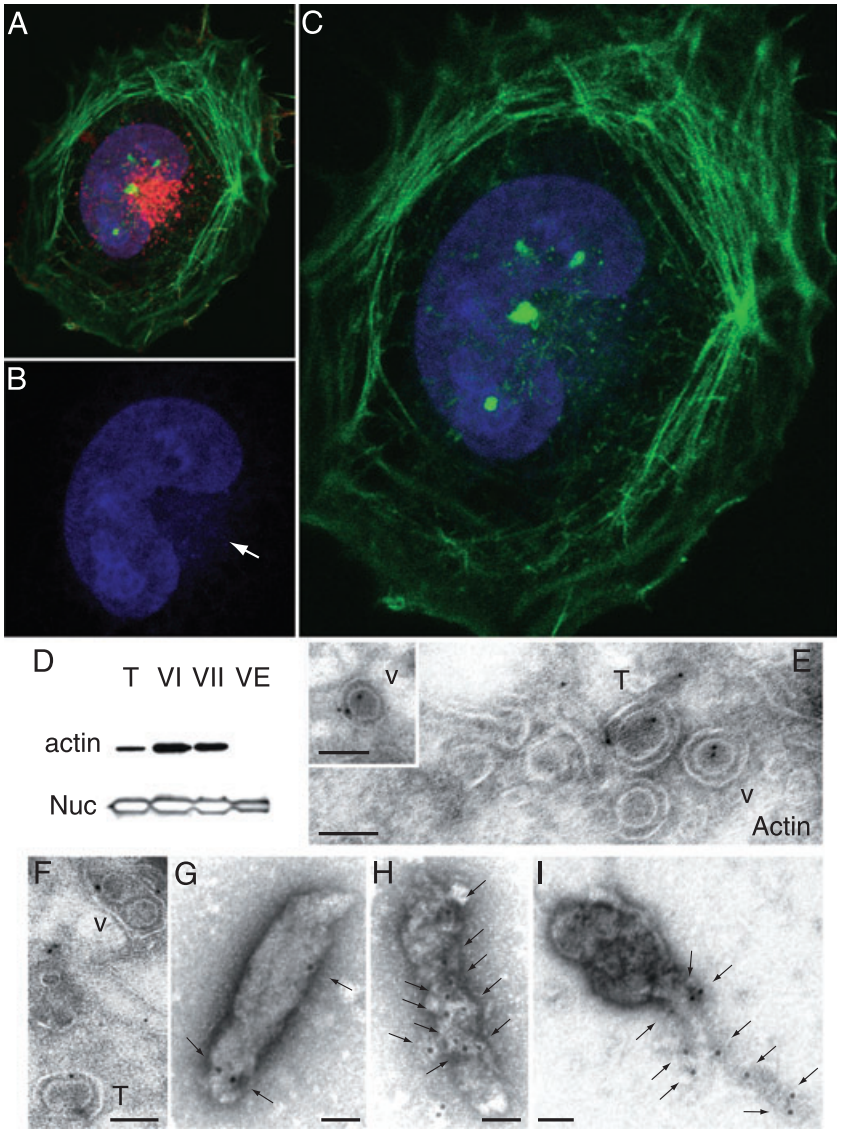

Fig. 5. Actin and viral tubes.
A. Confocal microscopy of viral factories shows a massive removal of stress fibres (Phalloidin, green) from the central areas of the cell and small spots of actin in the factory area coincident with Golgi staining (WGA, red).
B. Removal of red and green signals shows blue To-pro staining in nucleus and in the cytoplasmic factory area (white arrow).
C. Higher magnification and removal of red Golgi staining shows small, filamentous actin-containing elements in the factory. Z-series projections of single optical sections are shown in (A–C).
D. Western blot detection of actin in isolated tubes (T) and intracellular VI and VII viral forms, while no signal is detected in extracellular virions (VE). Detection of viral nucleocapsid (Nuc) was done in the same membrane.
E and F. Immunogold labelling on cryosections of infected cells showing actin-associated signal in viral particles (V) and the globular domain of viral tubes (T).
G–I. Immunogold detection of actin in isolated tubes treated with saponin. (G) Weak signal in intact tubes (arrows). (H) More intense signal in disrupted tubes (arrows). (I) Collapsed tubes with intense signals in released fibrous material (arrows). Bars: 100 nm in E and F; 50 nm in G–I.

assembled in Golgi stacks of cells treated with LtA, as observed in thin sections of treated cells studied by EM (not shown). However, treatment with Jpk led to a decrease in infectious virus release by 60–70% in cell cultures that simultaneously lose the actin stress fibres as observed by fluorescence microscopy (Fig. 6J and K). EM showed that in cells treated with Jpk cell organelles were displaced to the cell periphery against the plasma membrane (not shown) and Golgi fragments were occasionally distinguished (Fig. 6L). Intact viral tubes were not detected although their globular domains were seen in Golgi remnants (Fig. 6L) and attached to mitochondria (not shown). Viral assembly was massively displaced to the plasma membrane where budding profiles were frequently seen (Fig. 6M). Intracellular budding and viral particles in Golgi remnants were very scarce and observed exclusively in cells less affected by the drug according to characteristic Jpk effects in ultrastructure. Budding profiles were not distinguished at the plasma membrane of normally infected cells where budding events were exclusively located in Golgi stacks, as confirmed by analysis of oriented serial sections covering all planes from each infected cell. At least 200 cells per condition were studied.

Our results strongly support a functional participation of Golgi-associated actin in assembly and function of viral tubes as well as in anchoring virus assembly sites in Golgi membranes.

3D maps of early and late viral factories show viral tubes as the physical links between recruited cell organelles

As viral tubes could play multiple functions in bunyavirus

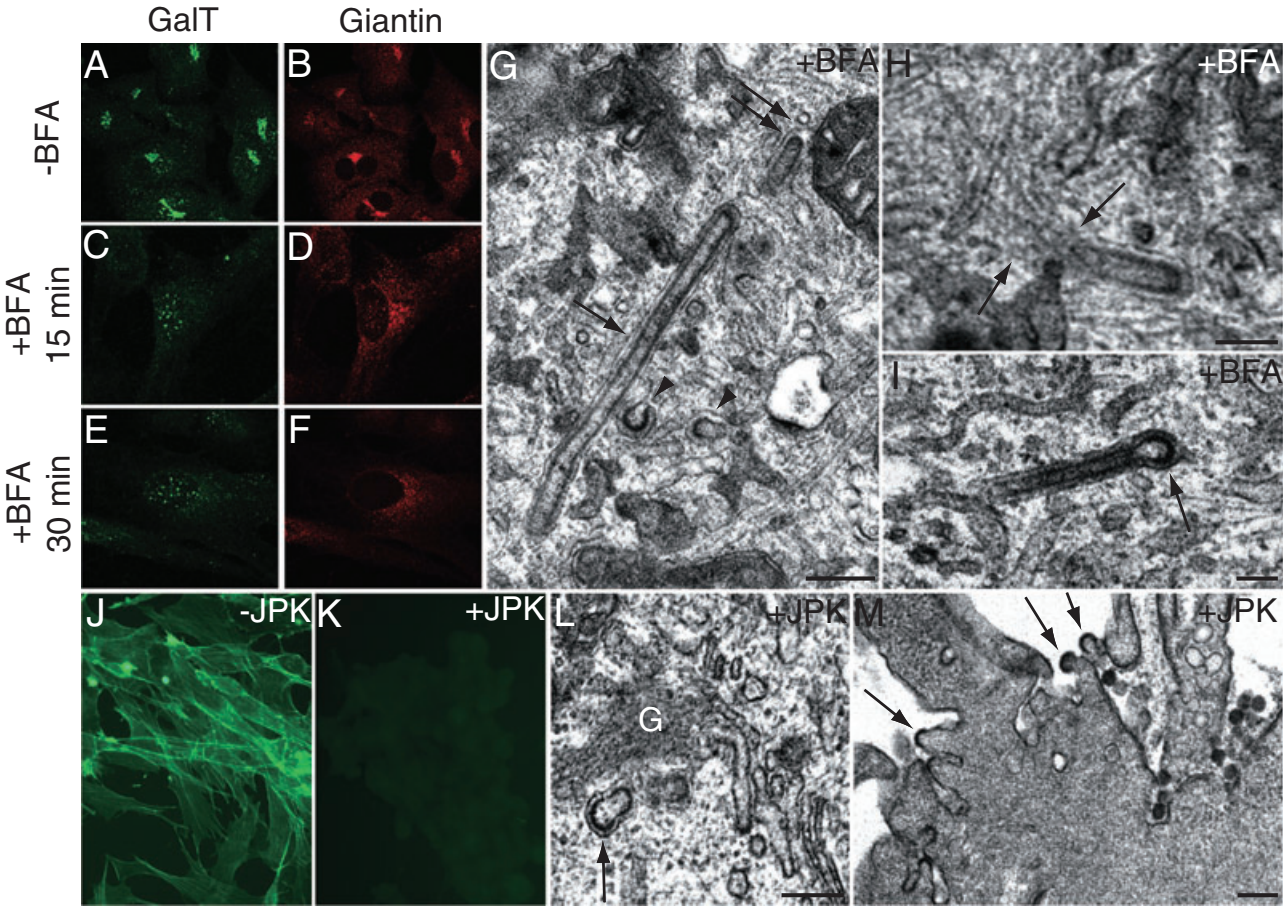

Fig. 6. Tube structure and virus assembly in the presence of drugs that affect Golgi membranes or actin integrity. Immunofluorescence microscopy of GalT and giantin in normally infected cells (5 PFU/cell) at 10 h p.i. (A and B), in infected cells treated 15 min with BFA (C and D) and in infected cells treated 30 min with BFA (E and F).
G and H. EM shows normal tubes out of Golgi stacks after 15 min with BFA.
G. Long tube (arrow) globular domains (arrowheads) and tube attached to mitochondria (double arrow).
H. Cytoplasmic filaments (arrows) apparently attached to a viral tube.
I. Normal tube with cylindrical and globular (arrow) domains after 30 min with BFA.
J and K. Fluorescence microscopy detection of actin (Phalloidin, green) in normally infected cells at 10 h p.i. (J) and in infected cells treated with JPK (drug was added at 1 h p.i.) (K).
L and M. EM of infected cells treated with JPK. Globular domain (arrow in L) in an altered Golgi stack (G) and budding profiles (arrows in M) in plasma membrane. Bars: 200 nm in G, L, M; 100 nm in H and I.

factories (replication, morphogenesis and organelle recruitment) a three-dimensional view of how they integrate in the factory and the contacts they establish with factory components can help us to understand how they work. We obtained serial sections of factories for a detailed study of the whole, complex structure. Analysis of all planes provided a much better characterization of factories compared with random planes with a more accurate quantification of numbers and dimensions of viral structures. Most tubes have a total length of 0.2–0.5 μm although tubes longer than 1 μm were occasionally seen. 3D reconstructions from serial sections were done for early (Fig. 7A–F) and late (Fig. 7G–I) factories. Early factories with few viral particles are round shaped structures near the nucleus and surrounded by mitochondria (Fig. 7A). A close-up of the central areas of this factory showed viral tubes that connect Golgi stacks with RER cisternae (Fig. 7B). The consecutive sections corresponding to these tubes are shown in Fig. 7C. This frequent contact was never detected after random analysis of factories in 2D which points to the importance of covering all the planes of very complex structures in an oriented manner. An important contact previously detected in 2D analysis occurred between tubes and mitochondria (Fig. 7D and E). Careful study of 3D maps revealed that early factories are indeed composed of repetitive units of a basic set integrated by a Golgi stack with mitochondria, RER and one or more viral tubes (Fig. 7F). By contrast, late factories are less compact structures that have abandoned the juxtanuclear location and contain many viral

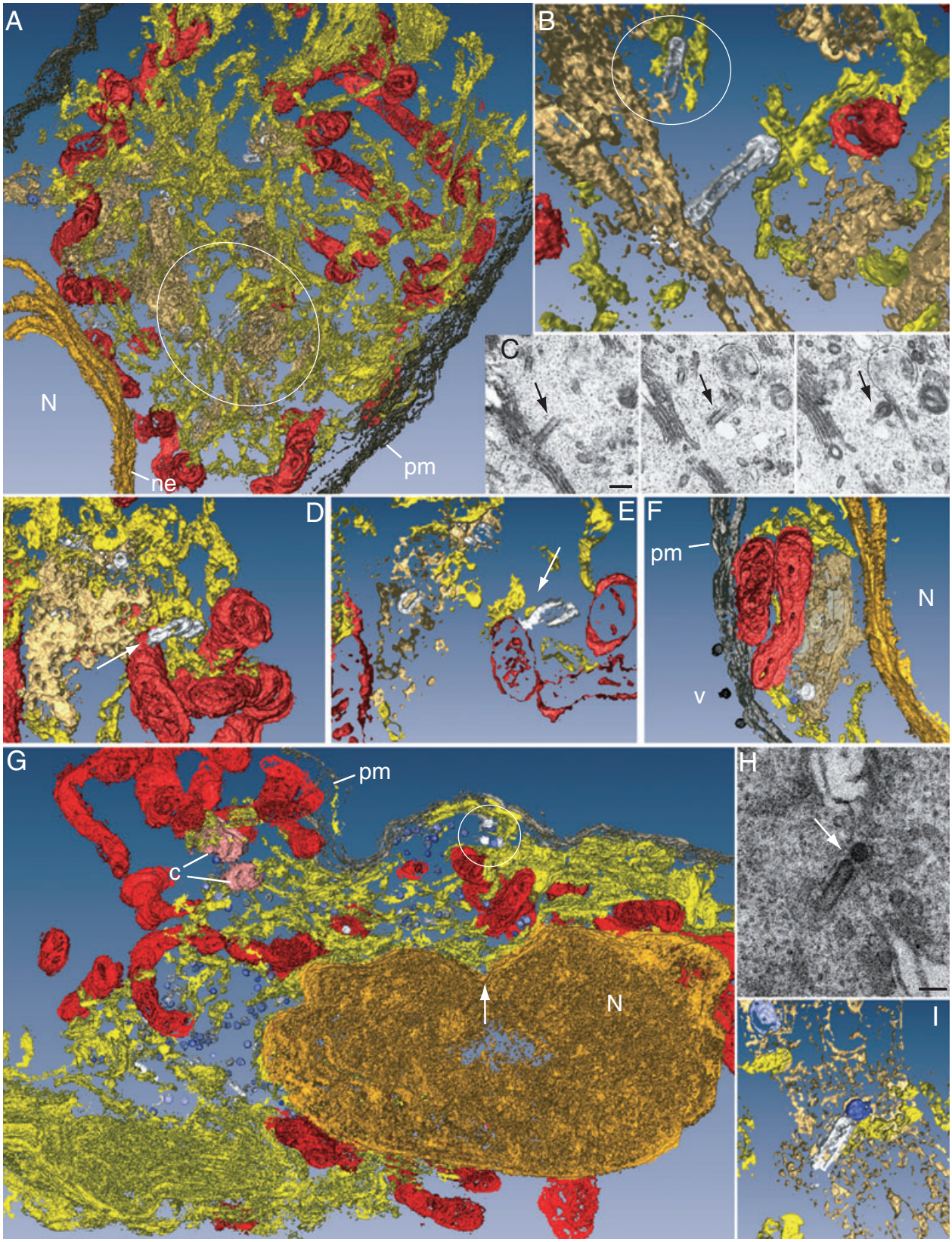

Fig. 7. 3D maps of early and late factories obtained by serial sectioning, TEM, 3D-reconstruction and image processing.
A. Large round-shaped early factory near the nucleus. Mitochondria (red) surround a network of membranes (yellow for the RER and beige for Golgi stacks) where viral tubes (grey) are embedded.
B. 3D reconstruction of the encircled central region of the factory in (A) elaborated with the central sections of the series to show contacts between viral tubes and cell membranes in more detail. The large tube is on the centre, a smaller one is encircled.
C. Three original serial thin sections included in the 3D map shown in (B). The central tube is marked with arrows.
D and E. Whole volume (D) and one single plane (E) of the same area of a factory showing a clear contact between a viral tube and a mitochondrion (arrows).
F. Basic factory unit constituted by a Golgi stack, RER elements, mitochondria and a viral tube. A viral particle is coloured in purple.
G. 3D map of a late factory. A significant displacement of components (mitochondria in red, RER in yellow) from the nuclear cavity (arrow) to peripheral areas of the cell is observed. Golgi-associated density has been omitted in this volume for better visualization of viral particles (purple). A contact between viral tubes (grey) and viral particles (purple) is encircled.
H and I. Original thin section and 3D reconstruction, respectively, of a viral tube touching a viral particle (arrow). N, nucleus; ne, nuclear envelope; pm, plasma membrane; v, extracellular virions; c, centrioles. Bar: 200 nm in C; 100 nm in H.

particles (Fig. 7G). Mitochondria and RER do not completely surround the factory and virus particles are moving towards the cell periphery. Physical contacts between viral tubes and new viral particles were detected as shown in the encircled area of Fig. 7G and in Fig. 7H and I. The existence of these contacts supports a role for the viral tubes as the physical connections between viral replication and morphogenesis inside the Golgi stacks of the virus factory as proposed in the model of Fig. 8.

Discussion

Viral factories are probably the most extreme examples of how viruses manipulate cell organization. It is remarkable that just a few different classes of viral macromolecular complexes can transform a whole eukaryotic cell in minutes. We are interested in understanding how this happens. At the same time, by studying viruses, we have a very valuable tool to study cell architecture.

In the present work we have characterized the bunyavirus factory built around the Golgi complex. Although the whole factory is large and complex it is in fact composed of repetitive units constituted by one or more Golgi stacks, mitochondria, RER elements and a tubular structure that acts as a link between these organelles. Further, the tubes could play multiple functions such as transfer of replicated viral genomes to assembly sites. Actin is needed both for assembly of these tubes and for virus morphogenesis in Golgi membranes. The presence of tubular structures in thin sections of mouse brain infected with BUNV was reported in old literature where they were interpreted as elongated virus particles or nucleocapsids (Murphy *et al.*, 1968). We also detected these structures in a previous study (Salanueva *et al.*, 2003) and estimated a discreet number of tubes, 2 or 3, per Golgi stack. Analysis of serial sections has provided us with a much more accurate appreciation of their real numbers, as all planes of the cell are analysed. As a consequence several new data have been obtained: tubes are in fact more abundant (more than 50 in many cells) and frequently connect with mitochondria and RER cisternae. Our structural characterization of viral tubes in Golgi membranes was completed with a molecular mapping of the structures both *in situ* and *in vitro* after their purification from infected cells. Identification of viral factors involved in genome replication and morphogenesis as well as cell proteins such as the translation elongation factor 2 or ribosomal proteins suggested that tubes may harbour

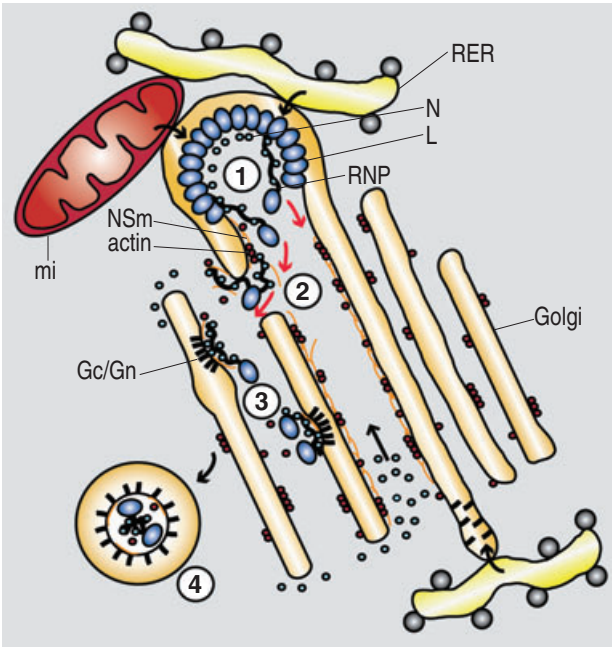

Fig. 8. Model for the functional structure of viral tubes integrated in the factory. Viral tubes assemble in association with Golgi membranes using endogenous actin and polymerized NSm as scaffold. Tubes attach to RER cisternae and mitochondria that provide cell factors needed for viral replication and assembly. Viral polymerase (L) concentrates in the globular domain. Replicated viral RNA (step 1) gets protected by interaction with N molecules, abundant around Golgi membranes and inside tubes. N molecules enter the tubes through their openings to the cytoplasm. With the help of actomyosin-based motors assembled RNPs then travel towards the cytoplasm (step 2), where they attach to the cytoplasmic domains of viral glycoproteins (Gc/Gn) concentrated in the nearby Golgi membranes. Budding events (step 3) lead to new viral particles that incorporate some amounts of the scaffold NSm protein and actin. Assembled immature viral particles are then ready for maturation and secretion (step 4).

post-replication events. A functional analysis of how altered NSm sequences or actin integrity affect factory architecture and viral assembly demonstrated that viral NSm protein and Golgi actin are essential for the structure and function of the tubes.

A sequence database comparison with BUNV NSm showed homology with NSm proteins from other bunyaviruses and a low (30%) similarity with human ATP P2X receptors. Immunoprecipitation assays showed that NSm interacts with N protein and the viral glycoproteins in infected cells (Shi *et al*., 2006). Interestingly, NSm from tospoviruses, the plant-infecting bunyaviruses, is a movement protein associated with transport of RNPs through plamodesmata (Storms *et al*., 1995). In mammalian cells tube-associated NSm could facilitate the transport of RNPs from the RCs to the assembly sites. Our data suggest that NSm could act also as a 'matrix' protein, facilitating binding of RNPs to the cytosolic domains of viral glycoproteins Gc and Gn in Golgi membranes. In fact its behaviour as a scaffolding protein that assists in viral assembly is supported by its presence in immature viral intermediates and its absence in mature extracellular virions. During tube assembly NSm aggregates seem to grow from the cytosolic side towards the interior of Golgi sacculi creating a new space (Fig. 1K). As *in situ* labelling experiments showed that actin and giantin are inside viral tubes when they are normally facing the cytosolic side of Golgi membranes, interactions of viral proteins with Golgi actin and matrix proteins could be essential for tube assembly.

Despite its highly organized structure the Golgi complex is a very dynamic organelle (James Morre and Mollenhauer, 2007). Nevertheless, the Golgi manages to maintain its high degree of structural organization thanks to a large group of Golgi-resident proteins that form a matrix. Various cytoskeletal networks together with coiled-coil proteins of the golgin family, such as the *cis*-golgins p115, GM130 and giantin, are components of this Golgi matrix (Short *et al*., 2005) that has been visualized by EM of detergent-extracted Golgi stacks (Fath and Burgess, 1993). Microtubules and associated motor proteins and the actin cytoskeleton are of particular importance in Golgi organization. Accordingly, several myosin motors localize to the organelle, where they are thought to contribute to the formation and transport of Golgi vesicles. Complex molecular machineries regulate actin dynamics involved in transport events in Golgi membranes (Fath *et al*., 1997; Beck, 2005).

Viruses manipulate actin in many different ways. They use actin for entry, intracellular transport, or cell-to-cell transmission (Pelkmans *et al*., 2002; Fackler and Krausslich, 2006; Radtke *et al*., 2006). Actin is involved in replication and transcription of both nuclear and cytoplasmic viruses and the infectious particles of retroviruses, herpesviruses, and picornaviruses contain actin (Grunewald *et al*., 2003; Radtke *et al*., 2006). When the actin cytoskeleton is destroyed with specific drugs a compaction of the Golgi complex is observed (Lazaro-Dieguez *et al*., 2006). Curiously, this altered Golgi is very similar to the round-shaped organelle we observed in BUNV factory whose assembly occurs simultaneously with relocation of stress fibres to the cell periphery (Fig. 1). In an attempt to test the potential function of actin in the structure and function of viral tubes we have used three actin-disrupting drugs. Two of them depolymerize filamentous actin (CyD and LtA) while the third one stabilizes filamentous actin (Jpk). Jpk stabilizes actin filaments *in vitro*, but *in vivo* it induces polymerization of monomeric actin into amorphous masses enhancing the rate of actin filament nucleation and disordered polymeric actin (Bubb *et al*., 2000). We used three drugs with different actin binding sites and different mechanisms of action because we wanted to target molecules associated to a very particular structure, the tubes inserted in Golgi stacks. Although we knew that viral tubes are open to the cytosol, we were not sure about efficiency and accessibility of drugs to actin molecules integrated in the tubular structure. In fact, while actin-depolymerizing drugs had little effect on viral tube structure and virus production, the F-actin-stabilizing drug Jpk altered the structure of viral tubes, the location of virus assembly sites and the release of infectious virus particles to the culture supernatants. Golgi-associated actin seems to play a structural role in maintaining the structural integrity of the viral tubes in Golgi membranes.

Brefeldin A is a drug that induces redistribution of most Golgi-localized proteins to the ER. Studies on the nature of the Golgi matrix scaffold showed that giantin, GM130, GRASP65 and GRASP55 end up in membranes called BFA remnants that are distinct from the ER (Seemann *et al*., 2000). These results supported the idea of a pre-existing template for Golgi stacks composed by these and other proteins. By using BFA we wanted to study if viral tubes disappear immediately when Golgi membranes fuse with the ER or if they stay for longer times following a common behaviour with the Golgi matrix scaffold. Like giantin viral tubes resisted short BFA treatments, which suggests they could be bound to the stable scaffold of Golgi stacks. Interestingly, integrity of Golgi actin and viral NSm protein is also important for viral tube structure and normal production of infectious virions. Our working hypothesis is that assembly of these viruses happens in Golgi membranes because replication machinery anchors in Golgi matrix components. A detailed study with silencing experiments and transfections with mutated components will be necessary to determine if particular Golgi matrix components are specifically involved in the organization and activities of viral tubes. Also to explore if myosin I molecules detected in isolated tubes are partici-

pating in transport of RNPs from the RCs to the assembly sites in nearby Golgi membranes.

According to our data, in particular the information coming from 3D maps and molecular detection, multiple interactions and movement of molecules must take place in viral tubes, as proposed in the working model of Fig. 8. Tubes represent a new structure that, in communication with the cytosol, would host viral RNA replication and assembly of RNPs in a protective environment, facilitating the posterior transfer of RNPs to the assembly sites. The unusual cylindrical shape of this viral RC-containing structure might be related with the organization of Golgi sacculi where viral tubes are anchored. Actin and other matrix proteins can form the cellular protein scaffold for NSm interactions and tube growth while the actomyosin-based motors might mediate macromolecular movements. Contacts with RER and mitochondria most probably provide necessary factors for tube functions. Future work aims to locate viral and cellular proteins in tubes after 3D reconstruction by electron tomography (Cyrklaff *et al*., 2005; McIntosh *et al*., 2005). Although factories are very large and complex structures for electron tomography we plan to use 3D maps from serial section reconstructions to assist in segmentation and interpretation of tomograms. In fact, our results also demonstrate that methods of 3D reconstruction from serial sections can benefit from the same principles of segmentation and noise reduction common to electron tomography. These procedures provide three-dimensional maps with enough resolution and details to analyse contacts between small elements such as virus assemblies inside very large and complex structures such as whole eukaryotic cells. This will hopefully help us to understand how viral macromolecular complexes interact with cell components to create the unique architecture of virus factories.

Experimental procedures

Cells, viruses, antibodies

BHK-21 (C13) cells supplied by the American Type Culture Collection (ATCC) were grown in Dulbecco's modified Eagle's medium supplemented with 10% foetal calf serum from Reactiva S.A. (Barcelona, Spain). BUNV (ATCC VR-87) was propagated and subjected to titre determination in BHK-21 cells by a lysis-plaque-forming assay, as previously described (Salanueva *et al*., 2003). BUNVs containing deletions in the gene for NSm protein and designated rBUNM-NSmΔ3 (aminoacids 354–400 were deleted from the M polyprotein), rBUNM-NSmΔ4 (deleted aminoacids, 377–426) and rBUNM-NSmΔ5 (deleted aminoacids, 410–456) were generated by reverse genetics as described (Shi *et al*., 2006). The MAB742 monoclonal antibody against *Bunyamwera* Gc glycoprotein, and an anti-NSm rabbit antiserum against the peptide TDQKYTLDEIADVLQA (residues 338–353 of the M segment precursor) were described previously (Watret *et al*., 1985; Nakitare and Elliott, 1993; Lappin *et al*., 1994). Rabbit antisera against the amino- and the carboxyl-terminal domains of viral L protein were previously characterized (Jin and Elliott, 1992). Rabbit anti-N antiserum was obtained by immunization with a synthetic peptide corresponding to the amino-terminal peptide of the protein (MIELEFHDVAANTSST) following standard procedures. The anti-giantin rabbit antiserum was a kind gift of M. Renz (Institute of Immunology and Molecular Genetics, Karlsruhe, Germany). Anti-β actin (clone AC-15) and A2668 rabbit anti-actin antiserum were from Sigma. Anti-Gal-T and anti-dsRNA K2 MAbs were kindly provided by T. Suganuma (Department Anatomy, Miyazaki Medical College, Japan) and N. Lukacs (Biological Research Center, Institute of Plant Biology, Szeged, Hungary), respectively. Anti-dsRNA J2 MAb was purchased from English and Scientific Consulting (Hungary). Anti-dsRNA antibodies have been validated as markers of viral replication for different RNA viruses (Schonborn *et al*., 1991; Westaway *et al*., 1999). Fluorescent secondary antibodies, Alexa 549, phalloidin (green), WGA (wheat germ agglutinin, red) and ToPro (marker for nuclei) were purchased from Molecular Probes/Invitrogen.

Infections and treatments with drugs

Monolayers of BHK-21 cells were infected with BUNV or NSm deletion mutant viruses at a multiplicity of infection (moi) of 1 or 5 plaque forming units (PFU) per cell. At 6, 8, 10 or 24 h p.i. culture supernatants were removed and cell monolayers processed for immunofluorescence or EM. Monolayers at 10 h p.i. were incubated 5, 15 or 30 min with culture medium containing 5 μg ml^{-1} BFA. For treatment with drugs for actin culture supernatants were removed at 1 h p.i. and substituted by medium with 2 μM CyD, 1 μM LtA or 0.5 μM Jpk. At 10 h p.i. cells were fixed and processed for microscopy.

Fluorescence and confocal microscopy

Cell monolayers grown on glass coverslips were fixed 20 min at 4°C with 4% paraformaldehyde in PBS before processing for immunolabelling of viral and cellular components as previously described (Novoa *et al*., 2005b; Fontana *et al*., 2007). A Zeiss Axiophot fluorescence microscope equipped with a MicroMax digital camera and a Bio-Rad Radiance 2100 confocal laser microscope were used for image collection.

Transmission electron microscopy

Cell monolayers were fixed 1 h at room temperature with a mixture of 1% glutaraldehyde and 0.5% tannic acid in HEPES buffer (pH 7.4) and processed by conventional embedding in the epoxy-resin EML-812 (Taab Laboratories) or in Lowicryl K4M (Taab) after cryo-processing by freeze-substitution as described (Fontana *et al*., 2007). Ultrathin sections (50–70 nm) were collected on cupper grids, stained with uranyl acetate and lead citrate or processed for immunogold labelling, and studied in a JEOL 1200-EX II electron microscope operating at 80 kv. Cryosections were obtained in an ultracryomicrotome (Leica EM FCS) operating at −120°C by the standard Tokuyasu method as described (Salanueva *et al*., 2003). For immunogold labelling primary antibodies were diluted in saturation buffer (PBS containing 1% BSA) as follows: 1:100 for anti-giantin, anti-L, anti-NSm

and rabbit anti-actin, 1:200 for anti-N and 1:50 for anti-dsRNA. Secondary antibodies conjugated with 10 nm colloidal gold particles from BBC were diluted 1:40 in the same buffer. Negative staining of isolated tubes and viruses was performed with uranyl acetate using standard procedures. For immunogold labelling samples adsorbed to EM grids were submitted to short incubations with primary and secondary antibodies before negative staining as described (Novoa *et al*., 2005b).

BrUTP labelling

The newly synthesized viral RNA in BUNV-infected BHK-21 cells was labelled from 4 to 5 h p.i. with 10 mM BrUTP (Sigma). At 1 h before labelling, 10 μg of actinomycin D (Sigma) per ml was added to the medium to block cellular RNA synthesis. BrUTP was introduced into cells using DOTAP Liposomal Transfection Reagent (Roche) as described (Westaway *et al*., 1999). Incubation with the mixture BrUTP-DOTAP-actinomycin D was maintained 1 h at 37°C. Cells were then washed with PBS, fixed with 4% paraformaldehyde + 0.05% glutaraldehyde in PBS and processed for cryosectioning and immunogold labelling using a monoclonal anti-bromodeoxyuridine antibody (Sigma) diluted 1:5 in saturation buffer followed by a secondary antibody-colloidal gold conjugate as described above.

Isolation and structural characterization of viral tubes

The established protocol for the isolation of intracellular viruses (Novoa *et al*., 2005b) was slightly modified for the purification of more labile structures such as the viral tubes. BHK-21 cells were infected at an moi of 3 PFU/cell and maintained 10 h at 37°C. Cells were washed and collected in TEN buffer containing protease inhibitors (Roche), and frozen at –80°C. After two consecutive cycles of freezing and thawing to release the viral tubes, cell lysate was clarified by centrifugation at 3700 *g*, 20 min at 4°C. Supernatant was centrifuged 2.5 h at 67 000 *g* through a 30% (w/v) sucrose cushion. Pellet was re-suspended in 150 μl of TEN with protease inhibitors and applied to a 15–25% (v/v) Optiprep iodixanol density gradient (Sigma). Centrifugation of samples was performed for 1.5 h at 250 000 *g*. Fractions of 250 μl were collected from the top of the gradient and processed for structural and biochemical characterization. Complete intact tubes localized in fractions 15–20 from the top, well separated from intracellular viral particles (fractions 27–38).

Controlled disruption of isolated tubes was done with saponin after adsorbing them on hydrophilic EM grids. Tubes were incubated with saponin (0.05% in PBS) during 15 s, 30 s or 1 min. After washing with PBS grids were processed for negative staining or immunogold labelling.

Biochemical analysis of isolated viral tubes: SDS-PAGE and Western blot

Purified viral tubes were processed by polyacrylamide gel electrophoresis (PAGE) in the presence of sodium dodecyl sulfate (SDS) with 8%, 11% or 14% acrylamide gels. Coomasie blue staining was used to visualize protein bands (Novoa *et al*., 2005b). For Western blot analysis proteins were transferred from gels to nitrocellulose membranes by standard blotting procedures. Membranes were saturated overnight at 4°C with PBS containing non-fat dry milk and 0.05% Tween 20, and incubated 1 h at room temperature with primary antibodies diluted in saturation buffer (1:200 for anti-L, 1:200 for anti-NSm and 1:200 for anti-β actin). After washing with this buffer, membranes were incubated with a horseradish peroxidase-conjugated secondary antibody diluted 1:2000. Immunoreactive bands were detected by chemiluminescence (ECL kit, Amersham).

For RNA dot-blotting samples were processed under RNase-free conditions as described (Brown *et al*., 2004). Samples were incubated overnight at 37°C in a mixture of 1 mg ml^{-1} proteinase K and 1% SDS in DEPC water. A positive control (dsRNA Birnavirus IBDV, E5 strain) kindly provided by Dr. D. Luque (CNB, Madrid), a negative control (yeast RNA from Sigma), purified extracellular BUNV virions and fractions enriched in intracellular viral tubes were applied to nitrocellulose membranes. Membranes were allowed to dry at room temperature during 15 min and processed for immunodetection of total RNA. After incubation with saturation buffer (5% dry milk in PBS) membranes were incubated 2 h with a mixture of J2 and K2 anti-dsRNA antibodies (diluted 1:100 each in saturation buffer), washed three times with the same buffer and incubated 1 h with a secondary antibody conjugated with horse radish peroxidase diluted 1:2000 in saturation buffer. After several washes in saturation buffer signal in membranes was visualized by chemiluminescence (ECL kit, Amersham).

Peptide mapping

Fractions containing tubes as detected by negative staining and EM and fractions without tubes were submitted to SDS-PAGE using 8% and 15% acrylamide gels to cover a wide molecular weight range. Exclusive bands in fractions containing viral tubes were processed by MALDI peptide mass fingerprinting and database searching as described (Navarro-Lerida *et al*., 2004).

Serial section 3D reconstruction

Ultrathin consecutive sections of approximately 50 nm were collected on Formvar-coated parallel-bar copper grids and stained with uranyl acetate and lead citrate and studied by EM. After selecting an interesting region in the series, photographs were taken at 25 000× magnification. Using an EPSON perfection Photo 3170 scanner the photographs were digitized at 300 dpi as 8-bit images with a final pixel size of 3.39 nm. The images were then normalized using the Bsoft software (Heymann and Belnap, 2007; http://lsbr.niams.nih.gov/bsoft/). Sections were aligned by selected traces between two consecutive sections using the free editor for serial section microscopy 'Reconstruct' (Fiala 2005; http://www.synapse-web.org/tools/index.stm/) taking into account the 'tips for aligning sections' of the User's manual. As sections had an average thickness of 50 nm the voxel in the serial section 3D reconstruction had an anisotropic size of 3.39 nm in XY axis and 50 nm in Z axis. Segmentation and 3D visualization were done with Amira (http://amira.zib.de). For noise-reduction, images were subjected to three iterations of a median filter (van der Heide *et al*., 2007). Isosurface was used for 3D visualization, and the optimal threshold for the different materials was determined using a previously implemented algorithm (Cyrklaff *et al*., 2005). Only elements with unequivocal identity

were included in the 3D representations. A total of 23 factories were studied by 3D reconstruction of serial sections and 15–20 sections per series were included. As individual sections have a thickness of 50–70 nm, the total thickness of the 3D maps in the Z axis was around 1 μm.

Acknowledgements

This work was supported by grants BMC2003-01630 and BFU2006-04584/BMC from the Ministerio de Educación y Ciencia of Spain (to C. Risco), JA-P06-TIC01426 and MEC-TIN2005-00447 (to J.J. Fernández) and Wellcome Trust Programme Grants 065121 and 079810 (to R.M. Elliott). Juan Fontana and Noelia López-Montero are recipients of contracts from the Comunidad de Madrid. We thank Sylvia Gutiérrez Erlandsson for expert support with confocal microscopy and Silvia Juárez for her support with peptide mass fingerprinting studies, Reyes Novoa and Gloria Calderita for technical assistance, Sonia Ruiz and Carmen López-Iglesias for support with cryosections, Xiaohong Shi for manuscript reading and Alberto Fraile-Ramos for helpful discussions and critically reading the manuscript.

References

Beck, K.A. (2005) Spectrins and the Golgi. *Biochim Biophys Acta* **1744:** 374–382.

Bridgen, A., Weber, F., Fazakerley, J.K., and Elliott, R.M. (2001) Bunyamwera bunyavirus nonstructural protein NSs is a nonessential gene product that contributes to viral pathogenesis. *Proc Natl Acad Sci USA* **98:** 664–669.

Brown, T., Mackey, K., and. Du, T. (2004) Analysis of RNA by Northern and slot blot hybridization. In *Current Protocols in Molecular Biology*. Ausubel, F.M., Brent, R., Kingston, R.E., Moore, D.D., Seidman, J.G., Smith, J.A., and Struhl, K. (eds). New York: John Wiley & Sons, Suppl 67, 4.9.1–4.9.1

Bubb, M.R., Spector, I., Beyer, B.B., and Fosen, K.M. (2000) Effects of Jasplakinolide on the kinetics of actin polymerization. *J Biol Chem* **275:** 5163–5170.

Cherry, S., Kunte, A., Wang, H., Coyne, C., Rawson, R.B., and Perrimon, N. (2006) COPI activity coupled with fatty acid biosynthesis is required for viral replication. *PloS Pathog* **2:** 900–912.

Cyrklaff, M., Risco, C., Fernandez, J.J., Jimenez, M.V., Esteban, M., Baumeister, W., and Carrascosa, J.L. (2005) Cryo-electron tomography of vaccinia virus. *Proc Natl Acad Sci USA* **102:** 2772–2777.

Elliott, R.M. (1990) Molecular biology of the Bunyaviridae. *J Gen Virol* **71:** 501–522.

Elliott, R.M. (1997) Emerging viruses: the Bunyaviridae. *Mol Med* **3:** 572–577.

Fackler, O.T., and Krausslich, H.G. (2006) Interactions of human retroviruses with the host cell cytoskeleton. *Curr Opin Microbiol* **9:** 409–415.

Fath, K.R., and Burgess, D.R. (1993) Golgi-derived vesicles from developing epithelial cells bind actin filaments and possess myosin-I as a cytoplasmically oriented peripheral membrane protein. *J Cell Biol* **120:** 117–127.

Fath, K.R., Trimbur, G.M., and Burgess, D.R. (1997) Molecular motors and a spectrin matrix associate with Golgi membranes in vitro. *J Cell Biol* **139:** 1169–1181.

Fiala, J.C. (2005) Reconstruct: a free editor for serial section microscopy. *J Microsc* **218:** 52–61.

Fontana, J., Tzeng, W.P., Calderita, G., Fraile-Ramos, A., Frey, T.K., and Risco, C. (2007) Novel replication complex architecture in rubella replicon-transfected cells. *Cell Microbiol* **9:** 875–890.

Grunewald, K., Desai, P., Winkler, D.C., Heymann, J.B., Belnap, D.M., Baumeister, W., and Steven, A.C. (2003) Three-dimensional structure of herpes simplex virus from cryo-electron tomography. *Science* **302:** 1396–1398.

Hagiwara, Y., Komoda, K., Yamanaka, T., Tamai, A., Meshi, T., Funada, R., *et al.* (2003) Subcellular localization of host and viral proteins associated with tobamovirus RNA replication. *EMBO J* **22:** 344–353.

van der Heide, P., Xu, X.P., Marsh, B.J., Hanein, D., and Volkmann, N. (2007) Efficient automatic noise reduction of electron tomographic reconstructions based on iterative median filtering. *J Struct Biol* **158:** 196–204.

Heymann, J.B., and Belnap, D.M. (2007) Bsoft: image processing and molecular modeling for electron microscopy. *J Struct Biol* **157:** 3–18.

Hobson, S.D., Rosenblum, E.S., Richards, O.C., Richmond, K., Kirkegaard, K., and Schultz, S.C. (2001) Oligomeric structures of poliovirus polymerase are important for function. *EMBO J* **20:** 1153–1163.

James Morre, D., and Mollenhauer, H.H. (2007) Microscopic morphology and the origins of the membrane maturation model of Golgi apparatus function. *Int Rev Cytol* **262:** 191–218.

Jin, H., and Elliott, R.M. (1992) Mutagenesis of the L protein encoded by Bunyamwera virus and production of monospecific antibodies. *J Gen Virol* **73:** 2235–2244.

Kopek, B.G., Perkins, G., Miller, D.J., Ellisman, M.H., and Ahlquist, P. (2007) Three-dimensional analysis of a viral RNA replication complex reveals a virus-induced mini-organelle. *PloS Biol* **5:** 2022–2034.

Lappin, D.F., Nakitare, G.W., Palfreyman, J.W., and Elliott, R.M. (1994) Localization of Bunyamwera bunyavirus G1 glycoprotein to the Golgi requires association with G2 but not with NSm. *J Gen Virol* **75:** 3441–3451.

Lazaro-Dieguez, F., Jimenez, N., Barth, H., Koster, A.J., Renau-Piqueras, J., Llopis, J.L., *et al.* (2006) Actin filaments are involved in the maintenance of Golgi cisternae morphology and intra-Golgi pH. *Cell Motil Cytoskeleton* **63:** 778–791.

Lyle, J.M., Bullitt, E., Bienz, K., and Kirkegaard, K. (2002) Visualization and functional analysis of RNA-dependent RNA polymerase lattices. *Science* **296:** 2218–2222.

Mackenzie, J. (2005) Wrapping things up about virus RNA replication. *Traffic* **6:** 967–977.

McIntosh, R., Nicastro, D., and Mastronarde, D. (2005) New views of cells in 3D: an introduction to electron tomography. *Trends Cell Biol* **15:** 43–51.

Murphy, F.A., Harrison, A.K., and Tzianabos, T. (1968) Electron microscopic observations of mouse brain infected with Bunyamwera group arboviruses. *J Virol* **2:** 1315–1325.

Nakitare, G.W., and Elliott, R.M. (1993) Expression of the Bunyamwera virus M genome segment and intracellular localization of NSm. *Virology* **195:** 511–520.

Navarro-Lerida, I., Martinez Moreno, M., Roncal, F., Gavilanes, F., Albar, J.P., and Rodriguez-Crespo, I. (2004) Proteomic identification of brain proteins that interact with dynein light chain LC8. *Proteomics* **4:** 339–346.

Nichol, S.T., Beaty, B., Elliott, R.M., Goldbach, R., Plyusnin, A., Schmaljohn, A.R., and Tesh, R.B. (2005) Bunyaviridae. In *Virus Taxonomy*. Fauquet, C.M., Mayo, M.A., Maniloff, J., Desselberger, U., and Ball, L.A. (eds). Amsterdam: Elsevier, pp. 695–716.

Novoa, R.R., Calderita, G., Arranz, R., Fontana, J., Granzow, H., and Risco, C. (2005a) Virus factories: associations of cell organelles for viral replication and morphogenesis. *Biol Cell* **97:** 147–172.

Novoa, R.R., Calderita, G., Cabezas, P., Elliott, R.M., and Risco, C. (2005b) Key Golgi factors for structural and functional maturation of bunyamwera virus. *J Virol* **79:** 10852–10863.

Pelkmans, L., Puntener, D., and Helenius, A. (2002) Local actin polymerization and dynamin recruitment in SV40-induced internalization of caveolae. *Science* **296:** 535–539.

Radtke, K., Dohner, K., and Sodeik, B. (2006) Viral interactions with the cytoskeleton: a hitchhiker's guide to the cell. *Cell Microbiol* **8:** 387–400.

Salanueva, I.J., Novoa, R.R., Cabezas, P., Lopez-Iglesias, C., Carrascosa, J.L., Elliott, R.M., and Risco, C. (2003) Polymorphism and structural maturation of bunyamwera virus in Golgi and post-Golgi compartments. *J Virol* **77:** 1368–1381.

Salonen, A., Ahola, T., and Kaariainen, L. (2005) Viral RNA replication in association with cellular membranes. *Curr Top Microbiol Immunol* **285:** 139–173.

Schonborn, J., Oberstrass, J., Breyel, E., Tittgen, J., Schumacher, J., and Lukacs, N. (1991) Monoclonal antibodies to double-stranded RNA as probes of RNA structure in crude nucleic acid extracts. *Nucleic Acids Res* **19:** 2993–3000.

Seemann, J., Jokitalo, E., Pypaert, M., and Warren, G. (2000) Matrix proteins can generate the higher order architecture of the Golgi apparatus. *Nature* **407:** 1022–1026.

Shi, X., Kohl, A., Leonard, V.H., Li, P., McLees, A., and Elliott, R.M. (2006) Requirement of the N-terminal region of orthobunyavirus nonstructural protein NSm for virus assembly and morphogenesis. *J Virol* **80:** 8089–8099.

Short, B., Haas, A., and Barr, F.A. (2005) Golgins and GTPases, giving identity and structure to the Golgi apparatus. *Biochim Biophys Acta* **1744:** 383–395.

Steven, A.C., Heymann, J.B., Cheng, N., Trus, B.L., and Conway, J.F. (2005) Virus maturation: dynamics and mechanism of a stabilizing structural transition that leads to infectivity. *Curr Opin Struct Biol* **15:** 227–236.

Storms, M.M., Kormelink, R., Peters, D., Van Lent, J.W., and Goldbach, R.W. (1995) The nonstructural NSm protein of tomato spotted wilt virus induces tubular structures in plant and insect cells. *Virology* **214:** 485–493.

Watret, G.E., Pringle, C.R., and Elliott, R.M. (1985) Synthesis of bunyavirus-specific proteins in a continuous cell line (XTC-2) derived from Xenopus laevis. *J Gen Virol* **66:** 473–482.

Westaway, E.G., Khromykh, A.A., and Mackenzie, J.M. (1999) Nascent flavivirus RNA colocalized *in situ* with double-stranded RNA in stable replication complexes. *Virology* **258:** 108–117.

Wileman, T. (2006) Aggresomes and autophagy generate sites for virus replication. *Science* **312:** 875–878.

